Successive change from band insulating phase to spin-singlet dimer phase in the pseudobrookite titanate $MgTi_2O_5$-Ti_3O_5 system

Daigo Indo,[1] Taisei Yoshinaga,[1] Mitsutoshi Arizono,[1] Kazuya Takasu,[1] Tetsuro Izaki,[1] Takumi Shirasaki,[2] Hinata Arai,[2] Hideki Kuwahara,[2] Kaoru Akimoto,[3] Kei Ikeda,[3] Takuro Katsufuji,[3] and Tetsuji Okuda[1,*]

[1]*Graduate School of Science and Engineering, Kagoshima University, Kagoshima 890-0065, Japan*

[2]*Department of Physics, Sophia University, Chiyoda-ku, Tokyo 102-8554, Japan*

[3]*Department of Physics, Waseda University, Tokyo 169-8555, Japan*

(Received 10 January 2024; accepted 6 May 2024; published 20 May 2024)

We have grown single crystals of mixed-valence pseudobrookite titanate $MgTi_2O_5$-Ti_3O_5 systems ($Mg_{1-x}Ti_{2+x}O_5$) and have systematically investigated their physical properties as a novel canonical mixed-valence system which shows a successive change from the nonmagnetic band insulating phase ($MgTi_2O_5$) to the charge-ordered spin-singlet dimer phase (Ti_3O_5). In comparison with $Al_{1-x}Ti_{2+x}O_5$ [R. Takahama *et al.*, Phys. Rev. Mater. **4**, 074401 (2020)], we have clarified that, in the lower x region of $Mg_{1-x}Ti_{2+x}O_5$, the physical properties are greatly affected by the change of electron density with a variation of x and we have found that the doped electrons enhance the optical conductivity along a Ti-Ti ladder direction. However, we have also clarified that, in the higher x region, almost all Ti^{3+} ions produced by an increase in x contribute not to an increase in itinerant electrons but to a development of Ti^{3+}-Ti^{3+} dimer correlation. These observations indicate a crossover from the conductance along the ladder direction to a nontrivial conductance under the background of the dimer correlation.

DOI: 10.1103/PhysRevB.109.205138

I. INTRODUCTION

Mixed-valence transition metal oxides often show various intriguing quantum phenomena [1] such as high-temperature superconductivity and colossal magnetoresistance. One such mixed-valence system is perovskite titanates $La_{1-x}Sr_{1-x}TiO_3$ [2] which is a mixed crystal system of antiferromagnetic Mott insulator $LaTiO_3$ and nonmagnetic band insulator $SrTiO_3$. This system shows diverse quantum phenomena: a Mott transition [2], superconductivity [3], quantum paraelectricity [4], large n-type thermoelectric response [5,6], and so on. Therefore, it is quite interesting to search for a novel quantum phenomenon in the related mixed-valence titanates.

In this paper, we have focused on a $MgTi_2O_5$-Ti_3O_5 system ($Mg_{1-x}Ti_{2+x}O_5$) as a novel mixed-valence titanate. One of the end compounds of this system, $MgTi_2O_5$, has an α-type pseudobrookite structure [shown in Fig. 1(b)] at room temperature (RT). The formal valence of the Ti ion in $MgTi_2O_5$ is tetravalence, so $MgTi_2O_5$ is a nonmagnetic band insulator. Another end compound, Ti_3O_5, has a β-type pseudobrookite structure [shown in Fig. 1(a)] at RT [7,8]. The formal valence of the Ti ion is $+3\frac{1}{3}$, so the magnetic Ti^{3+} ions ($3d^1$: $S = 1/2$) and nonmagnetic Ti^{4+} ions ($3d^0$: $S = 0$) exist at a ratio of 2:1. In the low-T β phase, at the same time as a Ti^{3+}/Ti^{4+} charge ordering, neighboring Ti^{3+} ions form a spin-singlet dimer, so Ti_3O_5 becomes a nonmagnetic insulator. As the temperature increases, the bulk Ti_3O_5 shows the successive structural phase transitions [9] from the β phase to the paramagnetic λ phase to the paramagnetic α phase. The structural phase transition from the β phase to the λ phase is a first-order structural phase transition accompanied by a large displacement of oxygen ions [9,10]. Recently, a reversible photoinduced phase transition between the β phase and the λ phase in nanocrystal Ti_3O_5 [10] and the anisotropic photoinduced phase transition in a single crystal [11] have been reported.

Recently, we succeeded in growing single crystals of the pseudobrookite $AlTi_2O_5$-Ti_3O_5 system, $Al_{1-x}Ti_{2+x}O_5$ [12]. We clarified the magnetic, transport, and thermoelectric properties and we found that, with an increase in x, the α, λ, and β phases successively appeared at RT. In this Al system, the λ phase just near the phase boundary between the λ and β phases was the most conductive one where the dimer correlation is much developed. We proposed that the dynamical correlation of the spin-singlet dimer may be realized in this conductive λ phase.

In order to understand the mixed-valence pseudobrookite titanates more deeply, we have grown single crystals of $Mg_{1-x}Ti_{2+x}O_5$ which has a wider range of formal valences of the Ti ion from $+4$ to $+3\frac{1}{3}$, and we have investigated their structural, magnetic, transport, thermoelectric, and optical properties. In comparison with $Al_{1-x}Ti_{2+x}O_5$, we have clarified that, in the lower x region of $Mg_{1-x}Ti_{2+x}O_5$, a picture of the electron-doped band insulator comes to the fore, so the physical properties are greatly affected by a change of electron density with x. We have found that in the lower x region, the itinerant electron mainly conducts along the ladder of the Ti-Ti pair. On the other hand, in the higher x region, a picture of the hole-doped dimer phase comes to the fore where the increased Ti^{3+} ions with an increase in x little contributes to

*okuda@eee.kagoshima-u.ac.jp

 ©2024 American Physical Society

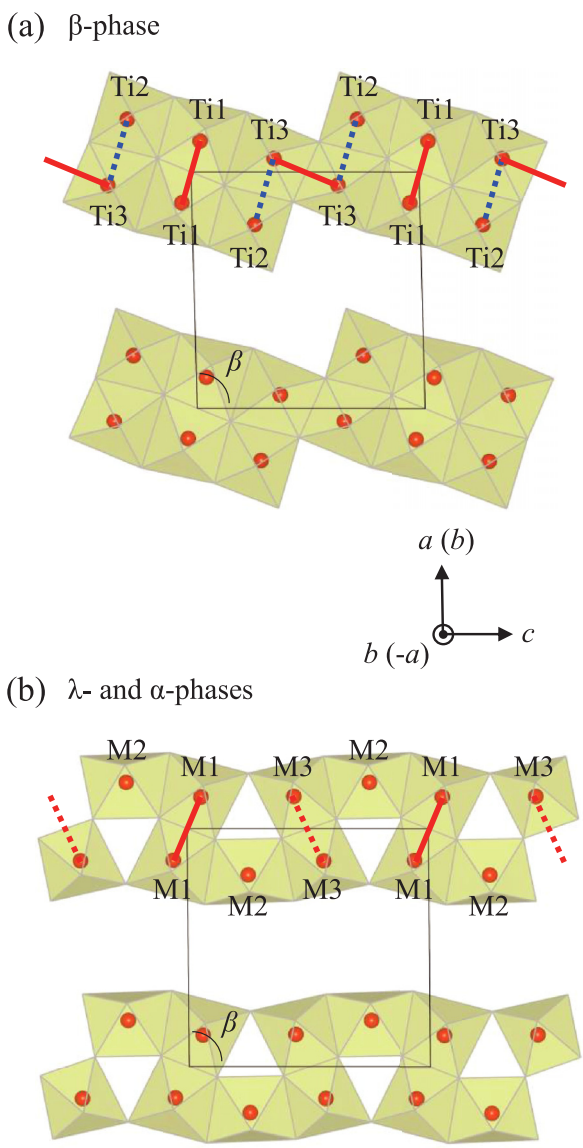

FIG. 1. Crystal structures of $Mg_{1-x}Ti_{2+x}O_5$ (a) in the β phase of Ti_3O_5 ($x = 1$) and (b) in the λ and α phases. In (a), the Ti1 and Ti3 sites are mainly occupied by Ti^{3+} ions and the Ti2 site is mainly occupied by the Ti^{4+} ions. M1, M2, and M3 in (b) show the virtual atoms partially occupied by Ti and Mg atoms. In the α phase, the β angle is 90° and the length between M1 and M1 atoms (solid lines) is equal to the length of M3 and M3 atoms (dashed lines). Tetragons in (a) and (b) show unit cells of the structures.

an increase in the itinerant electron but mainly contributes to a development of Ti^{3+}-Ti^{3+} dimer correlation which causes a nontrivial conductive phase under the background of the dimer correlation. These results support that $Mg_{1-x}Ti_{2+x}O_5$ is a novel canonical mixed-valence titanate system which shows a successive change from the nonmagnetic band insulating phase ($MgTi_2O_5$) to the charge-ordered spin-singlet dimer phase (Ti_3O_5).

II. EXPERIMENTAL PROCEDURE

Single crystals of $Mg_{1-x}Ti_{2+x}O_5$ were grown using a floating zone in an Ar gas for $x = 0$, in an Ar gas flow containing 0.5% H_2 gas for $0 < x \leqslant 0.5$, and in an Ar gas flow containing 7% H_2 gas for $0.5 < x \leqslant 1.0$. The seed materials were prepared by sintering the mixed starting materials of MgO (99.99%, Kojundo Co.) and TiO_2 (99.99%, Kojundo Co.) in air at 1000 °C for about 10 hours in the muffle furnace. The Mg contents determined by SEM-EDX measurements were almost consistent with the nominal values. Powder x-ray diffraction (XRD) measurements of the obtained crystals with Cu $K\alpha$ radiation indicated no impurity phase. The structural parameters were obtained via Rietveld analysis of the powder XRD profiles using RIETAN-FP [13]. The pictures of the structures shown in Figs. 1 and 12 are constructed using VESTA [14]. As an example, the XRD profiles and the data of the obtained structure parameters for $x = 0$ (α, $MgTi_2O_5$), 0.75 (λ), 0.9 (λ and β), and 1 (β, Ti_3O_5) are presented in Sec. A of the Supplemental Material [15].

A Quantum Design magnetic property measurement system (MPMS) was used to measure the T dependence of the magnetic susceptibility $\chi = M/H$ in a magnetic field of 0.5 T. The resistivity ρ at T below RT was measured with a four-probe method using a cryostat, while ρ and the Seebeck coefficient S were also measured from RT to about 1000 K with a four-probe method using an Advance RIKO ZEM-3 high-T thermoelectric measurement system. Some ρ-T curves showed discontinuities around RT because we changed the measurement system. Although we can correct to make the data connect smoothly, we have not in order to eliminate arbitrariness from deriving the thermoelectric power factor (PF) at high T. Furthermore, high-T data are absent for $x > 0.85$ because the crystals for $x > 0.85$ were so brittle and fragile that a large crystal could not be prepared for high T. The measurements for M, ρ, and S were done along the crystal growth directions. As discussed in the previous paper [12], the anisotropies in the physical properties were too small to detect in the α and λ phases of the psedobrookite titanates, although they should cause some measurement errors. Such a small anisotropy is partially evidenced by an absence of large anisotropy in a spectral weight of the low-energy optical conductivity in these phases, as shown in Fig. S8 [15]. Then, the observed distinct changes in physical properties with x in the α and λ phases were almost dominated by the changes in composition. As for the crystals having the line facets on the side in the β phase, the growth direction was observed to be nearly the $(0\ -1\ 1)$ direction.

Reflectivity measurement at RT was performed between 0.08 and 0.8 eV using an FTIR spectrometer and between 0.6 and 5.0 eV using a grating spectrometer on polished surfaces of the grown crystals. The axes of the crystals were determined by the Laue method. The optical conductivity spectra were obtained by the Kramers-Kronig transformation of the reflectivity spectra.

III. RESULTS AND DISCUSSION

A. Structural properties

Figure 2 shows the structural parameters of $Mg_{1-x}Ti_{2+x}O_5$ crystals (solid circles) obtained via Rietveld analysis of the powder XRD profiles (shown in Fig. S1 [15]) together with the reported parameters of polycrystalline $Mg_{1-x}Ti_{2+x}O_5$ (open

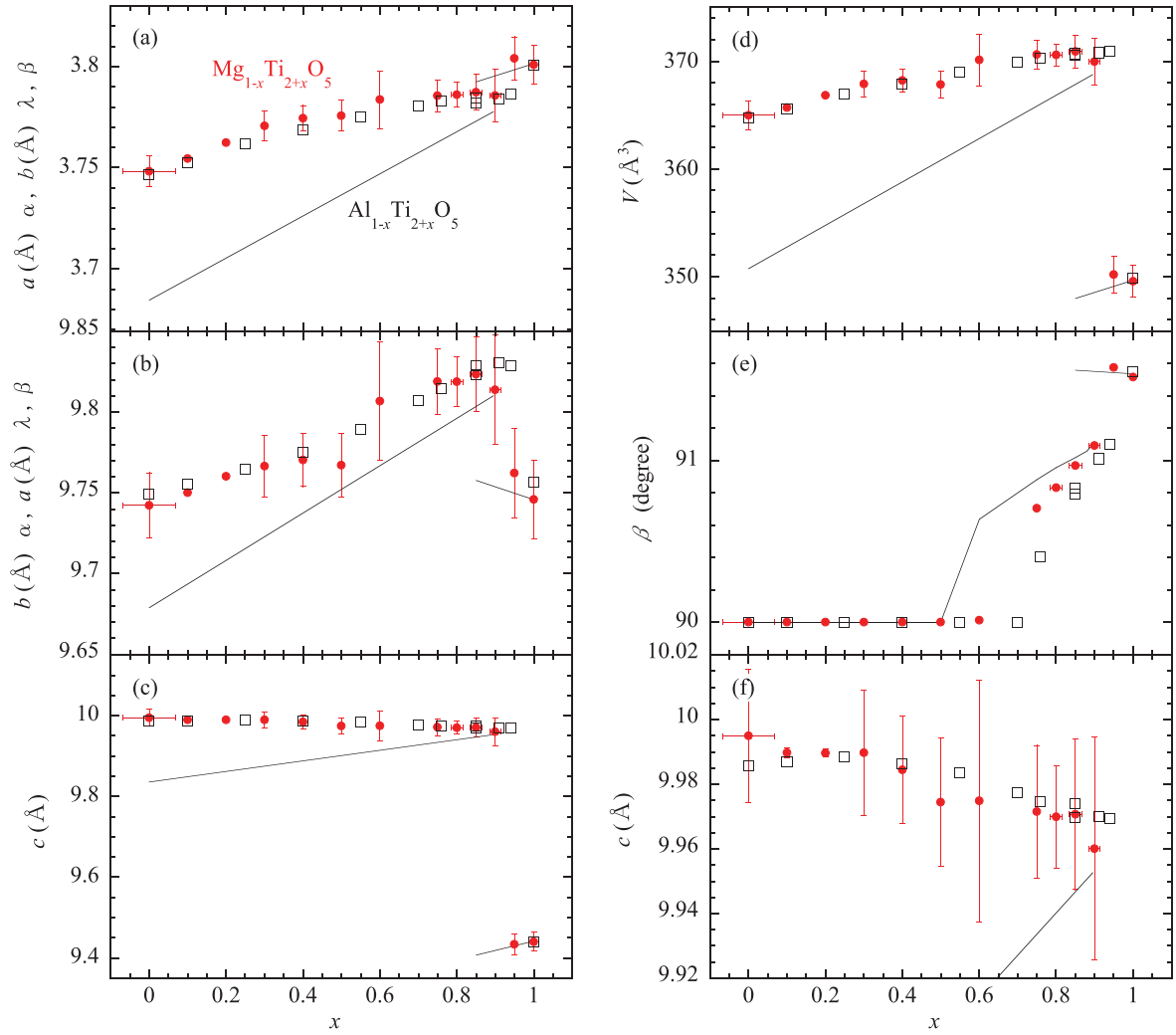

FIG. 2. Structural parameters at RT of $Mg_{1-x}Ti_{2+x}O_5$ together with those of $Al_{1-x}Ti_{2+x}O_5$. Closed symbols show the parameters of $Mg_{1-x}Ti_{2+x}O_5$ obtained via Rietveld analysis of the powder XRD profiles, while open symbols show the reported parameters of polycrystalline $Mg_{1-x}Ti_{2+x}O_5$ [16] and the solid lines show the parameters of $Al_{1-x}Ti_{2+x}O_5$ [12].

squares) [16] and those of $Al_{1-x}Ti_{2+x}O_5$ (solid lines) [12]. The obtained parameters of our crystals reproduced the reported ones of polycrystals. All lattice parameters and the unit cell volume of $Mg_{1-x}Ti_{2+x}O_5$ are larger than those of $Al_{1-x}Ti_{2+x}O_5$, perhaps because the size relation of ionic radii in the six-coordination is Mg^{2+} (0.72 Å) > Ti^{3+} (0.67 Å) > Ti^{4+} (0.605 Å) > Al^{3+} (0.535 Å). However, it cannot be explained by the ionic radii that, in the λ and α phases of $Mg_{1-x}Ti_{2+x}O_5$, the lattice parameters of the a and b axes and the unit cell volume V increase with an increase in x. The other factors such as the change of microscopic structure and structural symmetry which may be coupled with the dimer formation should be taken into account to explain the observations.

According to the powder XRD measurements, as well as in $Al_{1-x}Ti_{2+x}O_5$, all of the β, λ, and α phases appear at RT in $Mg_{1-x}Ti_{2+x}O_5$ with a change in x. Judging from the β angles shown in Fig. 2(e), the phase boundary between the α and λ phases in $Mg_{1-x}Ti_{2+x}O_5$ is at around $x = 0.6$ which a little deviates from that in $Al_{1-x}Ti_{2+x}O_5$ [12].

Figures 3(a) and 3(b) show the interatomic distances (Ti1-Ti1, M1-M1, and M3-M3 distances) for $Mg_{1-x}Ti_{2+x}O_5$ and $Al_{1-x}Ti_{2+x}O_5$, respectively. The M1, M2, and M3 atoms shown in Figs. 1(a) and 1(b) are the virtual atoms partially occupied by the Ti atoms and the Mg atoms. As shown in Fig. 3, the shortest interatomic distance is the one between the neighboring M1 atoms both in $Mg_{1-x}Ti_{2+x}O_5$ and in $Al_{1-x}Ti_{2+x}O_5$. For $Al_{1-x}Ti_{2+x}O_5$, the M1-M1 (or Ti1-Ti1) distances are always smaller than the Ti-Ti distance of a α-Ti metal (2.93 Å), while, for $Mg_{1-x}Ti_{2+x}O_5$, the M1-M1 distances are clearly smaller than the Ti-Ti distance of α-Ti metal only in the λ and β phases ($x > 0.5$). These observations seem to indicate that the Ti^{3+}-Ti^{3+} dimer correlation exists in all compositions for $Al_{1-x}Ti_{2+x}O_5$, while the dimer correlation significantly develops only for $x > 0.5$ for $Mg_{1-x}Ti_{2+x}O_5$.

Since, as shown in Fig. S2 [15], the M1-M1 distances of the Mg and Al systems seem to be well scaled by the number of d electrons per formula unit n_d, the dimer correlation is perhaps determined by n_d, regardless of the structural parameters and symmetry. On the other hand, the M1-M1 distance in

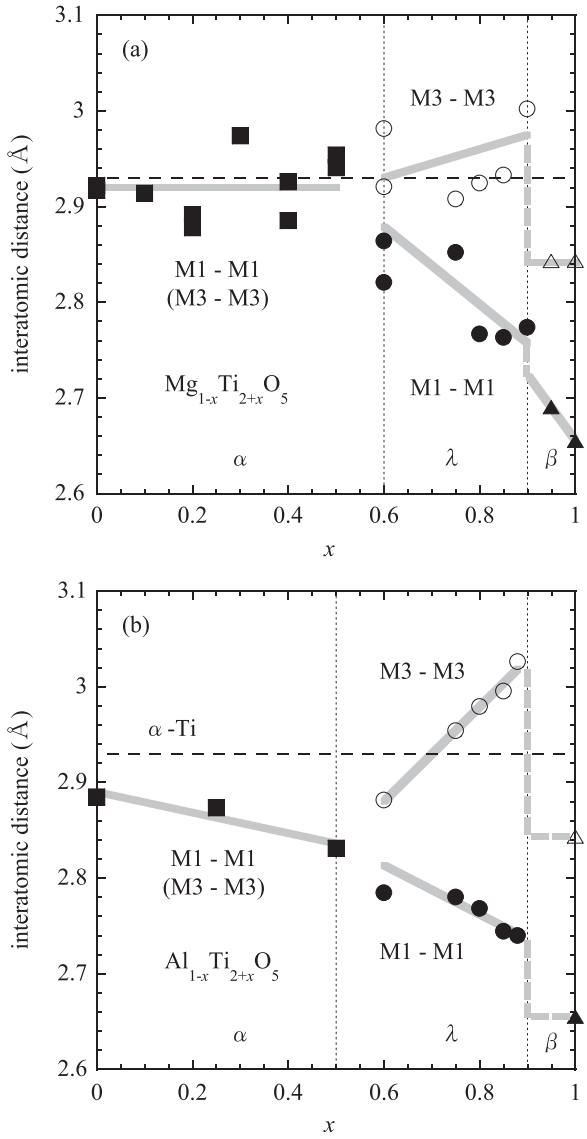

FIG. 3. Interatomic distances at RT for (a) $Mg_{1-x}Ti_{2+x}O_5$ and (b) $Al_{1-x}Ti_{2+x}O_5$ [12]. Horizontal dashed lines show the Ti-Ti distance of α-Ti metal and the vertical dashed lines show the approximate phase boundary between the α and λ phases and that between the λ and β phases. The closed squares show the M1-M1 distances in the α phase, the closed and open circles show the M1-M1 and M3-M3 distance in the λ phase, respectively, and the closed and open triangles show the M1-M1 and M3-M3 distance in the β phase, respectively. Thick solid and dashed lines are guides to the eye.

$Mg_{1-x}Ti_{2+x}O_5$ for $0 \leqslant x < 0.5$ ($0 \leqslant n_d < 1$) saturates at the values nearly equal to the Ti-Ti distance of a α-Ti metal and that of a rutile TiO_2 (2.96 Å), so the dimer correlation is not thought to develop so much in this composition region. This is apparently due to the small number of Ti^{3+} ions per formula unit ($n_d = 2x$). Suppose that the system is homogeneous and the dimer behaves like an orbital molecule. In that case, the probability that both neighboring dimer sites are occupied by Ti^{3+} ions is proportional to x^2 so it is rather small in the small x region [15]. Hence, the dimer correlation is not developed well in the small x region.

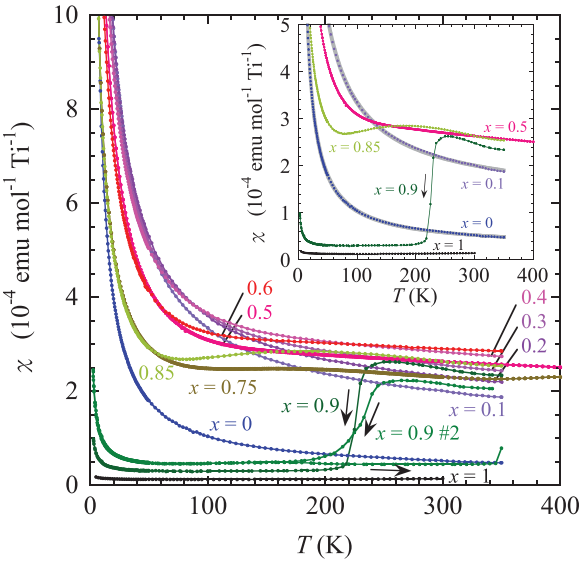

FIG. 4. T dependencies of magnetic susceptibilities χ (χ-T curves) of $Mg_{1-x}Ti_{2+x}O_5$ for $0 \leqslant x \leqslant 1$. The inset shows the magnifications of the χ-T curves for $x = 0$, 0.1, 0.5, 0.85, 0.9, 1.0. The result for $x = 0.9$ #2 is the result of the second measurement for $x = 0.9$. After the first measurement, the sample goes to pieces since it undergoes the first-order structural phase transition between the λ and β phases, so the transition becomes less sharp.

B. Magnetic properties

Figure 4 shows the T dependencies of magnetic susceptibilities (χ-T curves) of $Mg_{1-x}Ti_{2+x}O_5$ for $0 \leqslant x \leqslant 1$. Although the χ-T curves of $Mg_{1-x}Ti_{2+x}O_5$ are qualitatively similar to those of $Al_{1-x}Ti_{2+x}O_5$ [12], there are some differences originating from the expansion of the formal valence of the Ti ion. As shown in Fig. 5(a), for $0 \leqslant x < 0.4$, the χ at 300 K is clearly smaller than those for $Al_{1-x}Ti_{2+x}O_5$, which is apparently due to the differences of the formal valences of Ti ions. On the other hand, for $x \geqslant 0.4$, the χ at 300 K exhibits the saturating behavior with a change in x and it saturates at almost the same values of $Al_{1-x}Ti_{2+x}O_5$.

As shown in Fig. 4, the χ for $x < 1$ diverges at low temperatures. So the magnetic susceptibility below 20 K χ_{20K} is tentatively fitted by the following equation,

$$\chi_{20K} = \chi_C + \chi_0' = \frac{C}{T + \theta_C} + \chi_0', \tag{1}$$

where χ_C, C, θ_C, and χ_0' are the Curie-Weiss component, the Curie constant, the Curie-Weiss temperature, and the T-independent component, respectively. For $x < 0.4$, there seems to be another Curie-Weiss component and a more detailed analysis is presented in Sec. C of the Supplemental Material [15]. Figures 5(b) and 5(c) show the x dependencies of the θ_C and the ratio of the number of the isolated Ti^{3+} ions estimated from C to the number of Ti atoms $N(Ti^{3+})/N(Ti)$ ($\equiv r_C$), respectively. The χ_C for $x = 0$ ($MgTi_2O_5$) perhaps comes from some impurities and the θ_C is nearly zero within an experimental error, while the θ_C for $0 < x < 0.9$ is about 1 K. Since the compounds for $0 < x < 0.9$ have some electric conductivity as discussed later, the weak antiferromagnetic interaction via the itinerant carrier such as an RKKY interaction may exist. As shown in Fig. 5(c), the maximum absolute value

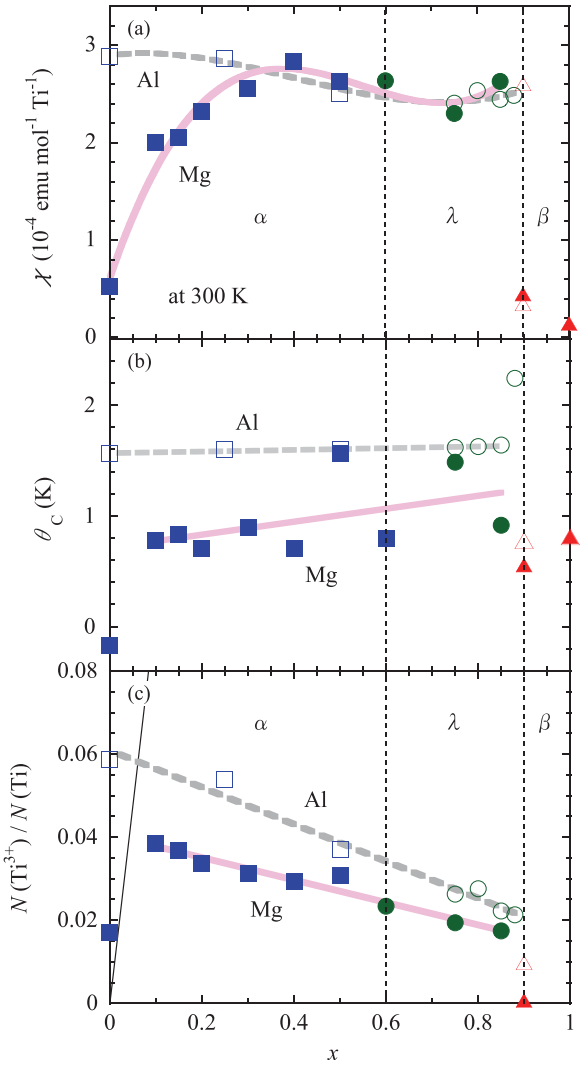

FIG. 5. x dependencies of (a) χ at 300 K, (b) Curie-Weiss temperature θ_C, and (c) the ratio of the number of Ti^{3+} ions deduced from the low-T χ and the number of Ti atoms $N(Ti^{3+})/N(Ti)$ ($\equiv r_C$) for $Mg_{1-x}Ti_{2+x}O_5$ (closed symbols) and $Al_{1-x}Ti_{2+x}O_5$ [12] (open symbols). The solid line in (c) shows the formal $N(Ti^{3+})/N(Ti)$ calculated from the formal valence of Ti ion. The closed squares, circles, and triangles represent the data for the α, λ, and β phases of $Mg_{1-x}Ti_{2+x}O_5$, respectively, and the open squares, circles, and triangles represent the data for the α, λ, and β phases of $Al_{1-x}Ti_{2+x}O_5$, respectively.

of r_C observed for $Mg_{1-x}Ti_{2+x}O_5$ is about 0.04 at $x \sim 0.1$ and, even if the second Curie-Weiss component r_{C2} is added [15], the maximum value of $r_C + r_{C2}$ will be about 0.07 as shown in Fig. S4(c) [15]. As for $Al_{1-x}Ti_{2+x}O_5$, it decreases monotonically as x increases. Since the $N(Ti^{3+})/N(Ti)$ estimated from the formal valence of the Ti ion are much larger than r_C or $r_C + r_{C2}$ [indicated by the solid line in Fig. 5(c)], it is speculated that almost all produced Ti^{3+} ions do not contribute to the isolated Ti^{3+} ion, but they contribute to the itinerant carrier or to the dimer formation. However, judging from the fact that the χ at 300 K saturates above $x = 0.4$ as shown in Fig. 4, it is thought that the contribution to the itinerant carrier saturates above $x = 0.4$ and almost all the Ti^{3+} ions contribute to the dimer formation in this composition region. In short, the dimer correlation is thought to much develop as the system approaches the β phase, which is consistent with the observation that the M1-M1 distance decreases as it approaches the β phase.

The development of the dimer correlation is also suggested by the T dependence of the χ. As shown in Fig. 4, the low-T χ for $x \geqslant 0.4$ is gradually suppressed as the system approaches the β phase and it shows the phase transition between the λ and β phases accompanying a hysteresis having a wide temperature range. When seeing the residual magnetic susceptibility $\chi - \chi_C$ shown in Figs. S3(a) and S3(b) of the Supplemental Material [15], the gradual suppression of the magnetic susceptibility is more clearly observed at low temperatures. For $x < 0.4$, the $\chi - \chi_C$ shows a monotonic behavior and it is well explained by the sum of the T-independent component χ_0 and the other Curie-Weiss component χ_{C2} having a higher Curie-Weiss temperature θ_{C2}. (See Sec. C of the Supplemental Material [15].) On the other hand, for $x \geqslant 0.4$, the $\chi - \chi_C$ shows nonmonotonic T dependence and it is gradually suppressed as x increases. Along with the saturation of χ at 300 K as x increases, these behaviors indicate that the spin-singlet Ti^{3+}- Ti^{3+} dimer correlation gradually develops at low temperatures as x increases.

C. Transport properties

1. Resistivity

Figure 6(a) shows the T dependencies of the resistivity (ρ-T curves) of $Mg_{1-x}Ti_{2+x}O_5$ for $x \leqslant 0.85$, together with the ρ-T curves of $AlTi_2O_5$ and $Al_{0.25}Ti_{2.75}O_5$ (solid lines). Although all compounds show insulating behaviors as in $Al_{1-x}Ti_{2+x}O_5$ [12], it can be seen that the range of change of ρ with respect to x is widening in comparison with $Al_{1-x}Ti_{2+x}O_5$. This is thought to be due to the expansion of the range of formal valences of the Ti ion from $+3\frac{1}{3} \sim +3.5$ to $+3\frac{1}{3} \sim +4$. Figure 7(a) shows the x dependence of ρ at 290 K for $Mg_{1-x}Ti_{2+x}O_5$ together with that for $Al_{1-x}Ti_{2+x}O_5$. For $x < 0.2$, the ρ for the Mg system is apparently larger than that for $Al_{1-x}Ti_{2+x}O_5$, reflecting the difference of the formal valence of Ti ions. However, for $x \geqslant 0.2$, a large discrepancy between the two systems is not observed. As discussed in Sec. III B, these behaviors are perhaps due to the following reasons: in the lower x region, the density of the itinerant carrier changes, reflecting the change of the formal valence of the Ti ion, but in the higher x region, the density saturates due to the fact that almost all Ti^{3+} ions additionally produced by an increase of x come to contribute to the Ti^{3+}-Ti^{3+} dimer formation and stop contributing to the physical properties. For $x > 0.3$, the ρ gradually decrease with an increase in x, which is perhaps because the disorder is suppressed due to the decrease of the impurities such as the isolated magnetic Ti^{3+} ions and the nonmagnetic Mg^{2+} ions, as discussed for $Al_{1-x}Ti_{2+x}O_5$ in the previous paper [12].

Figure 7(b) shows the x dependencies of the local activation energies E_a [$=d(\ln \rho)/dT^{-1}$] at 300 K and 800 K for $Mg_{1-x}Ti_{2+x}O_5$, together with those at 1000 K for $Al_{1-x}Ti_{2+x}O_5$. For $x < 0.2$, the clear difference between the two systems can be seen in the x dependence of the E_a at the

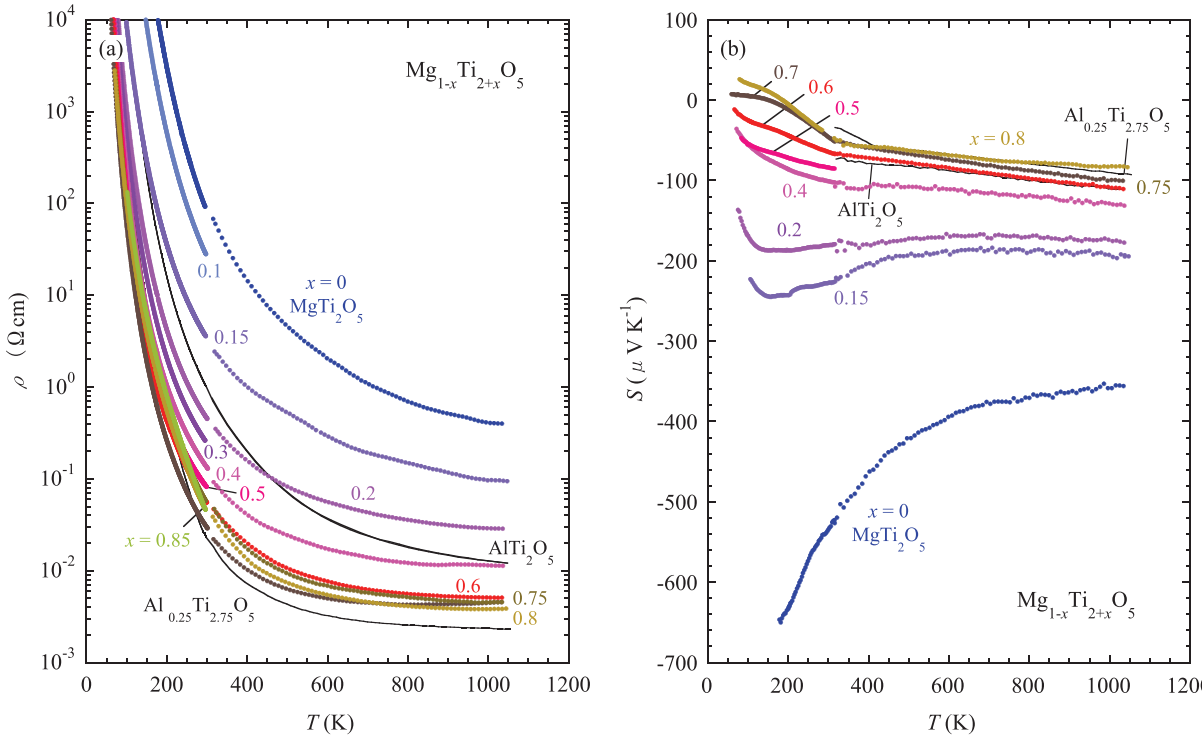

FIG. 6. T dependencies of (a) resistivity ρ and (b) Seebeck coefficients S of $Mg_{1-x}Ti_{2+x}O_5$ for $0 \leqslant x \leqslant 0.8$ together with $AlTi_2O_5$ and $Al_{0.25}Ti_{2.75}O_5$ (solid lines) [12].

high temperatures, as in that of the ρ at 290 K in Fig. 7(a), which perhaps originates from a difference of the electronic state. As can be seen from the fact that the E_a for $x < 0.2$ at 300 K and 800 K are almost the same value, the E_a for $x < 0.2$ are almost constant at above RT as shown in Fig. S5 [15], indicating that the electronic state $x < 0.2$ does not change with a variation of T from RT to the high T.

As for the x dependence, the E_a for $x \leqslant 0.2$ both at 300 K and 800 K monotonically decreases with an increase in x. This is because the number of carriers significantly increases with an increase in x. On the other hand, for $x > 0.2$, the E_a at 300 K and 800 K deviate with an increase in x, and the E_a at 300 K for $x \geqslant 0.5$ gradually increases with an increase in x toward the β phase despite that the ρ gradually decreases. It is presumed that such a behavior originates from the development of dimer correlation at low T which is indicated by the χ-T curves in Fig. 4. As shown in Fig. S5 [15], the E_a for $x = 0.8$ continuously increases as T decreases from 800 K which indicates that the dimer correlation remains at far above RT and it gradually develops as T decreases. It is thought that the itinerant carriers propagate in the background of the dimer correlation which develops with an increase in x or with a decrease in T. Such a carrier propagation may make the dimer correlation dynamic [17].

2. *Seebeck coefficient and thermal conductivity*

Figure 6(b) shows the T dependencies of Seebeck coefficients S of $Mg_{1-x}Ti_{2+x}O_5$ together with those of $AlTi_2O_5$ and $Al_{0.25}Ti_{2.75}O_5$. Comparing with $Al_{1-x}Ti_{2+x}O_5$, the variation of S with respect to x becomes considerably larger corresponding to the expansion of the range of the formal valence of the Ti ion. As shown in Fig. 6(b), except for in the low-T regime near the β phase, the sign of S is negative. In the high-T regime for $x = 0$, the S diverges roughly proportional to T^{-1} as T decreases perhaps due to the reduction of the thermal activated electrons. With an increase in x, the carrier density increases, so the absolute value of S dramatically decreases and shows a nearly metallic behavior in the higher x.

On the other hand, in the composition region near the β phase, the S-T curve shows a kink at the phase transition temperature between the α and λ phases [12], and as T decreases, the sign of S changes from negative to positive. It is thought that dimer correlation much develops in the region where S is positive, since the static dimer phases in some other dimer materials have been reported to show the p-type characteristics [18]. The electronic state of the region showing positive S can be regarded as the hole-doped dimer state as observed in Mg-doped Ti_2O_3 [19,20].

According to the shortest Ti-Ti distances in Fig. 3(a) and the χ-T curves in Fig. 4 and Fig. S3 [15], there is a gradual development of dimer correlation as x increases, while electrons are doped into the band insulating state. This means that as the system approaches the β phase, it is in a mixed state of an electron-doped state and a hole-doped dimer state at low temperatures. Since the contributions of electrons and holes to the Seebeck coefficients cancel each other out, as shown in Fig. 6(b), the Seebeck coefficient becomes small at low temperatures as x increases, even though the highly insulating nature is maintained.

Figure 7(c) shows the x dependencies of S at 1000 K for $Mg_{1-x}Ti_{2+x}O_5$ and $Al_{1-x}Ti_{2+x}O_5$. As well as in the cases of

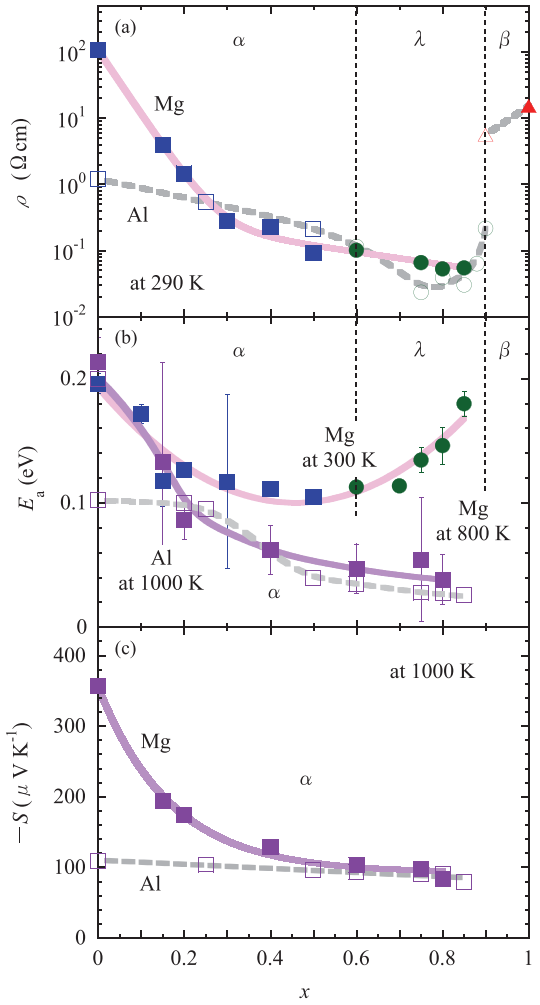

FIG. 7. x dependencies of (a) the resistivity ρ at 290 K, (b) the local activation energy E_a at 300 K and 800 K, and (c) Seebeck coefficients S at 1000 K for $Mg_{1-x}Ti_{2+x}O_5$ together with (a) ρ at 290 K, (b) E_a at 1000 K, and (c) S at 1000 K for $Al_{1-x}Ti_{2+x}O_5$ [12]. The symbols are the same as those in Fig. 5.

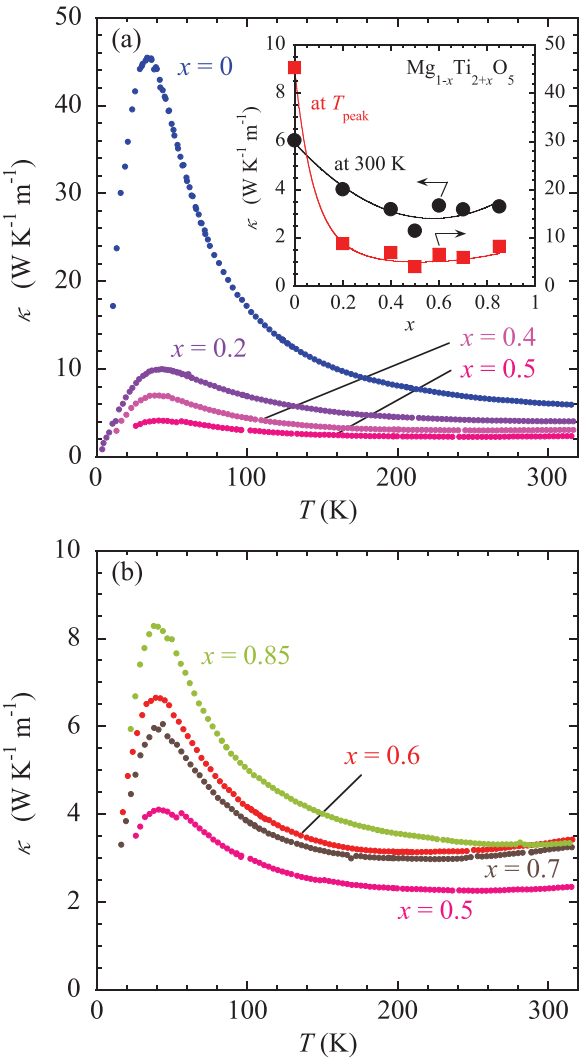

FIG. 8. Thermal conductivities κ of $Mg_{1-x}Ti_{2+x}O_5$ below RT for (a) $0 \leqslant x \leqslant 0.5$ and (b) $0.5 \leqslant x \leqslant 0.85$. The inset of (a) shows x dependencies of κ at RT and the peak temperature T_p.

other physical properties such as χ and ρ, there is a large difference in S at 1000 K for $x < 0.4$, but, when $x \geqslant 0.4$, the S values almost saturate and there is little difference between $Mg_{1-x}Ti_{2+x}O_5$ and $Al_{1-x}Ti_{2+x}O_5$. Taking into account the small difference in E_a at high temperatures between the two systems for $x \geqslant 0.4$, it is thought that, in spite of the different formal valences of Ti ions, there is not much difference in the electronic states near the Fermi level in both systems for $x \geqslant 0.4$; i.e., most Ti^{3+} ions contribute to a development of the dimer correlation and they do not contribute to an increase in itinerant electrons.

As well as in the case of $Al_{1-x}Ti_{2+x}O_5$, $Mg_{1-x}Ti_{2+x}O_5$ shows the best thermoelectric PF at around $x = 0.75$ where there is little difference in ρ and S between the two systems. Then, the observed maximum PF for $Mg_{1-x}Ti_{2+x}O_5$ is about 2 $\mu W\,K^{-2}\,cm^{-1}$ at 1000 K for $x = 0.75$ which is the same as that of $Al_{1-x}Ti_{2+x}O_5$ [12] within the experimental errors, as shown in Fig. S6 [15].

As shown in Fig. 8, the thermal conductivities κ for all compositions show peaks at around 40 K. The κ for $x = 0$ ($MgTi_2O_5$) shows a nearly typical peak structure which can be explained by the product of lattice specific heat and relaxation time that takes into account contributions of scattering of various boundaries, point defects, and umklapp scattering. As shown in the inset of Fig. 8(a), the κ at the peak temperature T_p is largely suppressed with an increase in x to 0.2. The dramatic decrease of κ is perhaps due to an increase of point defect caused by excess Ti ions. Above $x = 0.2$, κ gradually decreases with an increase in x, takes a minimum value at around $x = 0.5$, and begins to increase above $x = 0.5$. The slight increase of κ at T_p with an increase in x from 0.5 to 0.85 may be due to the decrease of the Mg ion with an increase in x toward another end compound Ti_3O_5 or due to a gradual hardening of the lattice originating from a gradual development of the dimer correlation. The κ at RT in the x region from 0.2 to 0.85 are 2–4 $W\,K^{-1}\,m^{-1}$ which are close to the typical values of thermoelectric materials. If the $x = 0.75$ compound takes a

similar value of κ at 1000 K, the thermoelectric figure of merit ZT is estimated to be 0.05–0.1.

D. Optical properties

Figures 9(a)–9(e) show the optical conductivity spectra $\sigma(\omega)$ along the a (a'), b (b'), and c axes for $Mg_{1-x}Ti_{2+x}O_5$ with (a) $x = 0$ ($MgTi_2O_5$), (b) $x = 0.2$, (c) $x = 0.5$, (d) $x = 0.75$, and (e) $x = 1$ (Ti_3O_5) at RT. Figures 10(a) and 10(b) show the $\sigma(\omega)$ spectra for $Al_{1-x}Ti_{2+x}O_5$ with (a) $x = 0$ ($AlTi_2O_5$) and (b) $x = 0.75$, which was previously reported [11]. The a' and b' axes of the α phase correspond to the b and a axes, respectively, of the same phase so that the same direction of the crystal is given by the same character for all of the α, λ, and β phases.

In the $\sigma(\omega)$ spectra for $x = 0$ ($MgTi_2O_5$) along all three directions shown in Fig. 9(a), only a small spectral weight was observed below 3 eV. Since this compound, if stoichiometric, is a d^0-band insulator, this may be due to a contribution of the d electrons produced by nonstoichiometry of the sample. As shown in Figs. 9(a)–9(c) and Figs. S7(a)–S7(c) [15], with an increase in x from 0 to 0.5, the spectral weight of $\sigma(\omega)$ below 3 eV monotonically increases for all three directions. Figure 11 shows the spectral weight of $\sigma(\omega)$ along the a, b, and c axes up to 1.5 eV [D_a(1.5 eV), D_b(1.5 eV), and D_c(1.5 eV)] and 2.5 eV [D_a(2.5 eV), D_b(2.5 eV), and D_c(2.5 eV)] as a function of the number of d electrons per formula unit, n_d. As can be seen, D_a(1.5 eV), D_b(1.5 eV), D_c(1.5 eV) and D_a(2.5 eV), D_b(2.5 eV), D_c(2.5 eV) monotonically increase with an increase in n_d from 0 ($x = 0$) to 1 ($x = 0.5$).

On the other hand, as shown in Figs. 9(a)–9(e), the $\sigma(\omega)$ spectra along the b axis below 1.5 eV are rather suppressed with increasing x more than 0.5, whereas the $\sigma(\omega)$ spectra along the a and c axes keep developing with increasing x up to $x = 1$. This is more clearly seen in the n_d dependence of the spectral weight shown in Fig. 11. Namely, D_b(1.5 eV) and D_b(2.5 eV) have a maximum at $n_d = 1$ ($x = 0.5$), whereas the D_a(2.5 eV), D_c(1.5 eV), and D_c(2.5 eV) monotonically increase with increasing n_d up to 1.5 ($x = 0.75$). Note that D_a(1.5 eV) is suppressed at $n_d = 2$ in the β phase since the spectral weight around 1 eV is transferred to ~2 eV due to the dimer formation, as shown in Fig. 9(e). In Fig. 11, the result for $Al_{1-x}Ti_{2+x}O_5$ is also plotted, where D_b is always smaller than the D_a and D_c and monotonically increases with increasing n_d up to 1.75 ($x = 0.75$).

As discussed in the previous sections, since the Ti^{3+}-Ti^{3+} dimer correlation barely develops in a small x region due to the small number of Ti^{3+} ions, a picture of "an electron-doped band insulator" is valid in this regime. As shown in Fig. 12, a ladder structure of Ti-Ti pairs exists along the a (b') axis of the α phase and the b axes of the λ and β phases in the pseudobrookite structure, and it can cause the conduction of the electrons along the ladder direction, resulting in the enhancement of the $\sigma(\omega)$ spectra along the b axis below 1.5 eV and D_b with increasing x up to 0.5, as shown in Figs. 9 and 11. Note that such an electronic conduction along the ladder direction has been qualitatively reproduced by the first-principles calculation for the λ phase of Ti_3O_5 [21]. As discussed in Sec. C of the Supplemental Material [15], the second Curie-Weiss component of the magnetic susceptibility perhaps originates from the magnetic interaction between the localized spins mediated by this electron conduction along the ladder direction. Experimentally, however, with further increasing x, the $\sigma(\omega)$ spectra along the b

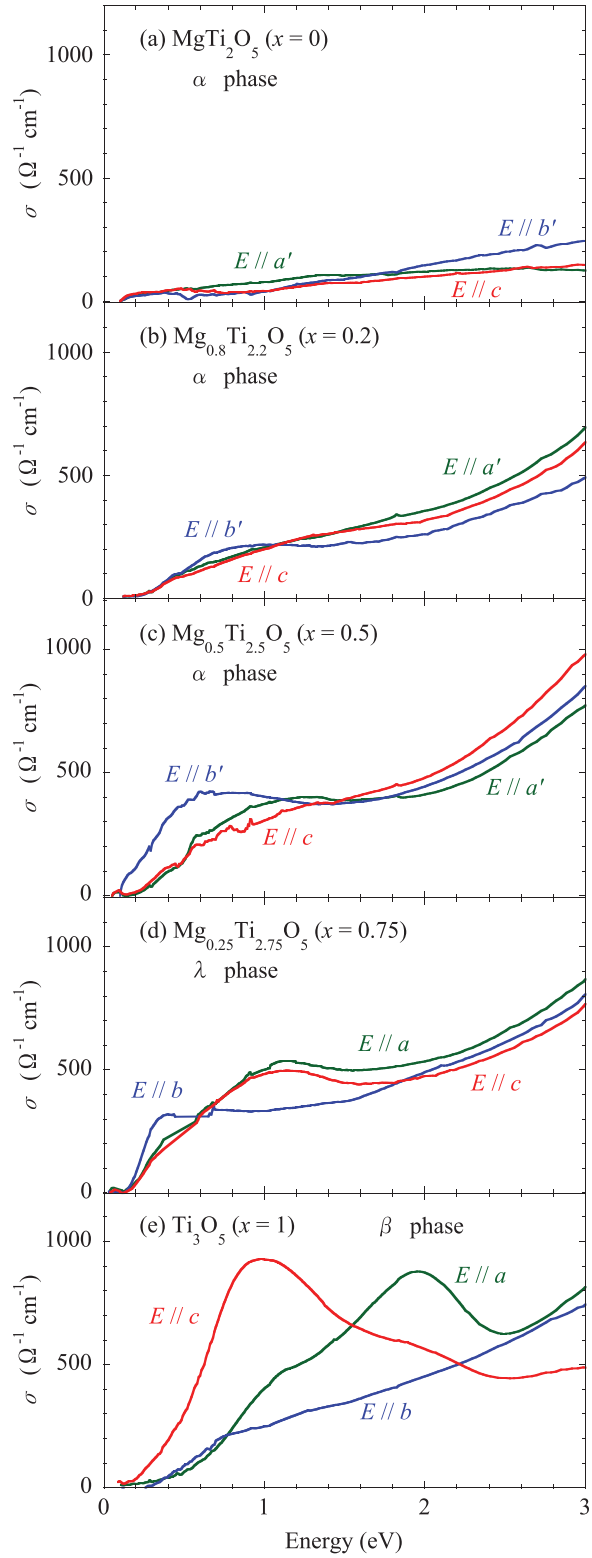

FIG. 9. Optical conductivity spectra $\sigma(\omega)$ for (a) $MgTi_2O_5$, (b) $Mg_{0.8}Ti_{2.2}O_5$, (c) $Mg_{0.5}Ti_{2.5}O_5$, (d) $Mg_{0.25}Ti_{2.75}O_5$, and (e) Ti_3O_5 [11]. In (a), (b), and (c), the a' and b' axes represent the b and a axes of the α phase, respectively.

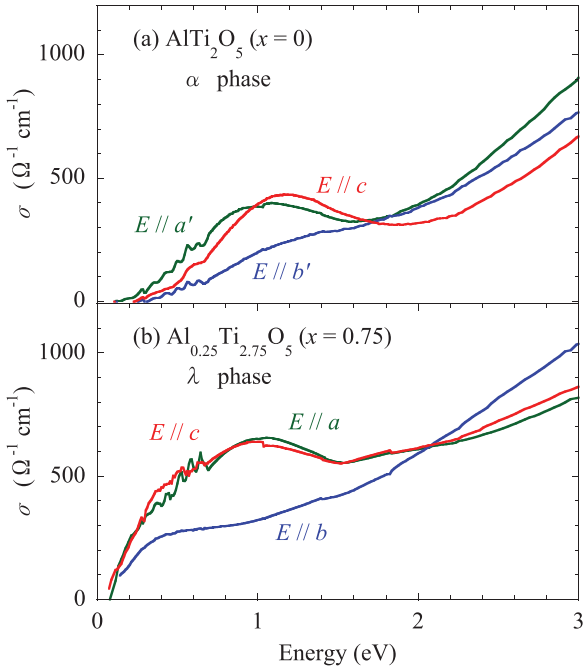

FIG. 10. Optical conductivity spectra $\sigma(\omega)$ [11] for (a) $AlTi_2O_5$ and (b) $Al_{0.25}Ti_{2.75}O_5$. In (a), the a' and b' axes represent the b and a axes of the α phase, respectively.

axis and D_b decrease, as shown in Figs. 9 and 11. This is likely due to the development of the Ti^{3+}-Ti^{3+} dimer correlation, which causes the localization of the d electrons within the ac plane and reduces their conduction along the b axis in the λ and β phases.

As discussed in Ref. [11], the peak at 1 eV for the $\sigma(\omega)$ spectrum along the c axis for the β phase of Ti_3O_5 can be assigned to the excitation of the d electron in the bonding state of the Ti dimer along the c axis to the antibonding state of the Ti dimer along the a axis, and the peak at 2 eV of the $\sigma(\omega)$ spectrum along the a axis can be assigned to the excitation of the d electron in the bonding state of the Ti dimer along the a axis to the antibonding state of the same dimer. It is likely then that the peak at 1 eV in the $\sigma(\omega)$ spectra along the a and c axes for $Mg_{1-x}Ti_{2+x}O_5$ with $0.5 \leqslant x \leqslant 0.75$ is due to the excitation of the d electron between the bonding state to the antibonding state of the Ti dimer shown in Fig. 1(b). The appearance of such a peak for $x \geqslant 0.5$ suggests the localization of the d electrons and the development of the dimer correlation within the ac plane of the λ phase (the bc plane of the α phase) in this x range. This is consistent with the fact that the $\sigma(\omega)$ spectra along the b axis below 1.5 eV are suppressed in this x range.

It should be also pointed out that D_a and D_c are barely different between $Mg_{1-x}Ti_{2+x}O_5$ and $Al_{1-x}Ti_{2+x}O_5$ with a comparable $n_d = 1$, but the D_b(1.5 eV) and D_b(2.5 eV) for $Al_{1-x}Ti_{2+x}O_5$ with $n_d = 1$ are much smaller than those for $Mg_{1-x}Ti_{2+x}O_5$ with the same n_d, as shown in Fig. 11. Note that even if n_d is the same, the number of substituted ions, $1 - x$, for $Al_{1-x}Ti_{2+x}O_5$ is larger than that for $Mg_{1-x}Ti_{2+x}O_5$, and thus the ladder structure is subject to a larger amount of disorder for the Al series. Such a disorder introduced by substitution may result in the suppression of the electron

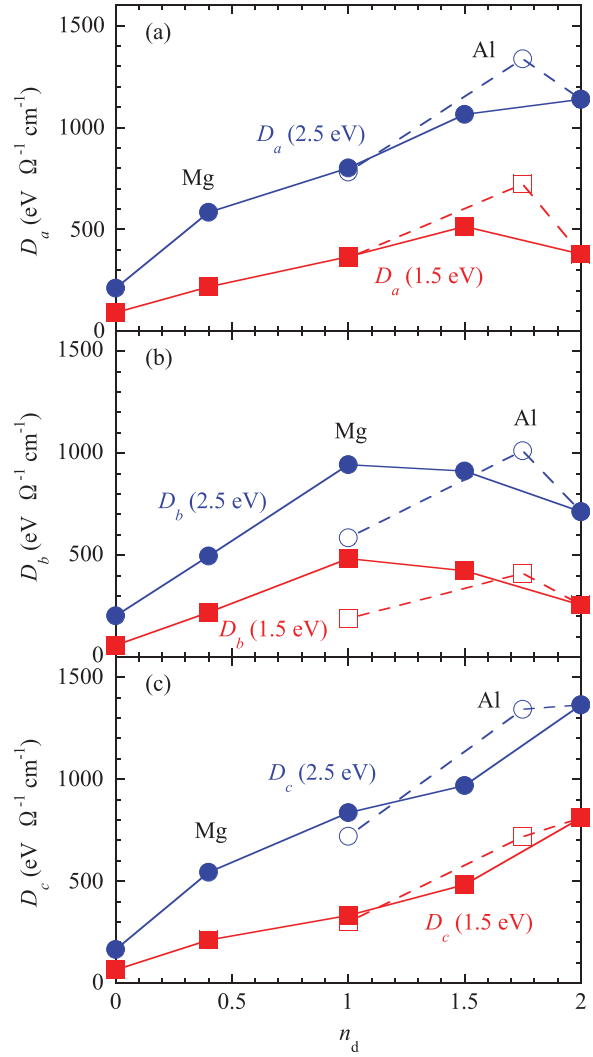

FIG. 11. Number of d-electron (n_d) dependencies of spectral weights of $\sigma(\omega)$. (a) $D_a(\epsilon_c)$ expresses the spectral weights with $E \parallel a$ in the λ and β phases and $E \parallel a'$ (b) in the α phase, (b) $D_b(\epsilon_c)$ with $E \parallel b$ in the λ and β phases and $E \parallel b'$ (a) in the α phase, and (c) $D_c(\epsilon_c)$ with $E \parallel c$ in all the phases. ϵ_c is an upper limit of energy integral.

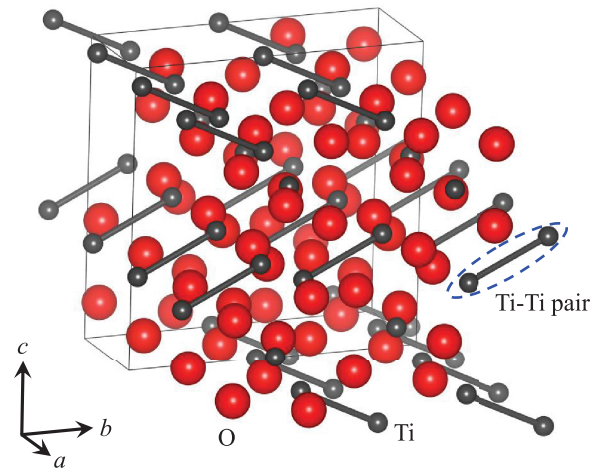

FIG. 12. Ladder structure of Ti-Ti pairs of α-$Mg_{0.5}Ti_{2.5}O_5$ ($x = 0.5$) along the a (b') axis.

conduction along the b axis and a significant decrease in D_b for $Al_{1-x}Ti_{2+x}O_5$. It is likely that such disorder barely affects the spectral weight for the excitation from the bonding state to the antibonding state in the Ti dimer, resulting in the comparable values of D_a and D_c between the Al series and the Mg series.

IV. SUMMARY

In this paper, we have grown single crystals of the mixed-valence pseudobrookite titanate $MgTi_2O_5$-Ti_3O_5 system ($Mg_{1-x}Ti_{2+x}O_5$) and have systematically investigated their physical properties as a novel canonical mixed-valence system which shows a successive change from the nonmagnetic band insulating phase ($MgTi_2O_5$) to the charge-ordered spin-singlet dimer phase (Ti_3O_5).

Comparing with $Al_{1-x}Ti_{2+x}O_5$ [12], in the lower x region, the distinct differences in the physical properties have been observed between the Mg and Al systems, and the optical conductivity σ_b along the direction of the Ti-Ti ladder has been observed to be enhanced. On the other hand, in the higher x region, the physical properties such as magnetic susceptibility χ at 300 K, resistivity ρ at 290 K, and Seebeck coefficient S at 1000 K are almost saturated with respect to x and there is almost no difference in them between the two systems, although the M1-M1 distances for both systems are gradually shortened with an increase in x and there are some differences in structural parameters between the two systems. In this composition region, σ_b is suppressed, while the optical conductivities σ_a, σ_c in the plane where the Ti^{3+}-Ti^{3+} dimers lie gradually develop with an increase in x.

These observations are interpreted as follows. In the lower x region, the physical properties are governed mainly by the change of the carrier (electron) density corresponding to the formal valences of Ti ions and the doped electrons primarily conduct through the Ti-Ti ladders which enhances σ_b and perhaps causes the second Curie-Weiss component of the magnetic susceptibility. In the higher x region, almost all produced Ti^{3+} ions no longer contribute to an increase in the electron density but to a development of the dimer correlation, which is partially manifested by a lack of large changes of various physical properties with respect to x, by the change of the sign of S from negative to positive with approaching β phase where the static dimer phase is stabilized, and by the enhancements of σ_a and σ_c. There must be a crossover from a conductance along the Ti-Ti ladder to a unique conductance under the background of the dynamical dimer correlation like a spin liquid.

ACKNOWLEDGMENTS

We thank Prof. T. Saitoh and N. Hamada for helpful discussions. This work was supported by the Japan Society for the Promotion of Science (KAKENHI Grant No. 21K03474), and was partly carried out at the Joint Research Center for Environmentally Conscious Technologies in Materials Science (Project No. 02315, Grant No. JPMXP0723833151) at ZAIKEN, Waseda University.

[1] M. Imada, A. Fujimori, and Y. Tokura, Rev. Mod. Phys. **70**, 1039 (1998).
[2] Y. Tokura, Y. Taguchi, Y. Okada, Y. Fujishima, T. Arima, K. Kumagai, and Y. Iye, Phys. Rev. Lett. **70**, 2126 (1993).
[3] J. F. Schooley, W. R. Hosler, and M. L. Cohen, Phys. Rev. Lett. **12**, 474 (1964).
[4] K. A. Müller and H. Burkard, Phys. Rev. B **19**, 3593 (1979).
[5] T. Okuda, K. Nakanishi, S. Miyasaka, and Y. Tokura, Phys. Rev. B **63**, 113104 (2001).
[6] S. Ohta, T. Nomura, H. Ohta, and K. Koumoto, J. Appl. Phys. **97**, 034106 (2005).
[7] S. Åsbrink and A. Magnéli, Acta Cryst. **12**, 575 (1959).
[8] L. N. Mulay and W. J. Danley, J. Appl. Phys. **41**, 877 (1970).
[9] M. Onoda, J. Solid State Chem. **136**, 67 (1998).
[10] S. Ohkoshi, Y. Tsunobuchi, T. Matsuda, K. Hashimoto, A. Namai, F. Hakoe, and H. Tokoro, Nat. Chem. **2**, 539 (2010).
[11] T. Saiki, T. Yoshida, K. Akimoto, D. Indo, M. Arizono, T. Okuda, and T. Katsufuji, Phys. Rev. B **105**, 075134 (2022).
[12] R. Takahama, T. Ishii, D. Indo, M. Arizono, C. Terakura, Y. Tokura, N. Takeshita, M. Noda, H. Kuwahara, T. Saiki, T. Katsufuji, R. Kajimoto, and T. Okuda, Phys. Rev. Mater. **4**, 074401 (2020).
[13] F. Izumi and K. Momma, Solid State Phenom. **130**, 15 (2007).
[14] K. Momma and F. Izumi, J. Appl. Cryst. **44**, 1272 (2011).
[15] See Supplemental Material at http://link.aps.org/supplemental/10.1103/PhysRevB.109.205138 for the XRD profiles, the structural parameters, the interatomic bond lengths, the magnetic susceptibilities, the local activation energy, the thermoelectric power factors, and the optical conductivities.
[16] I. E. Grey, C. Li, and I. C. Madsen, J. Solid State Chem. **113**, 62 (1994).
[17] P. W. Anderson, Mater. Res. Bull. **8**, 153 (1973).
[18] J. M. Honig and T. B. Reed, Phys. Rev. **174**, 1020 (1968); S. H. Shin, G. V. Chandrashekhar, R. F. Loehman, and J. M. Honig, Phys. Rev. B **8**, 1364 (1973).
[19] K. Takasu, M. Arizono, T. Shirasaki, H. Arai, H. Kuwahara, T. Yoshida, T. Katsufuji, and T. Okuda, JPS Conf. Proc. **38**, 011116 (2023).
[20] T. Miyoshino, D. Takegami, A. Meléndez-Sans, R. Nakamura, M. Yoshimura, K.-D. Tsuei, K. Takasu, T. Okuda, L. H. Tjeng, and T. Mizokawa, Phys. Rev. B **107**, 115145 (2023).
[21] C. Mariette, M. Lorenc, H. Cailleau, E. Collet, L. Guérin, A. Volte, E. Trzop, R. Bertoni, X. Dong, B. Lépine, O. Hernandez, E. Janod, L. Cario, V. Ta Phuoc, S. Ohkoshi, H. Tokoro, L. Patthey, A. Babic, I. Usov, D. Ozerov, L. Sala, S. Ebner, P. Böhler, A. Keller *et al.* Nat. Commun. **12**, 1239 (2021).